# Spin fluctuations in random magnetic-nonmagnetic two-dimensional antiferromagnets. II. Heisenberg percolation

R. J. Birgeneau*
*Department of Physics and Center for Materials Science and Engineering, Massachusetts Institute of Technology, Cambridge, Massachusetts 02139*

R. A. Cowley,† G. Shirane, and J. A. Tarvin‡
*Brookhaven National Laboratory, Upton, New York 11973*

H. J. Guggenheim
*Bell Laboratories, Murray Hill, New Jersey 07974*

(Received 9 July 1979)

In this paper we report an extensive study using neutron scattering techniques of the spin fluctuations in the two-dimensional diluted near-Heisenberg antiferromagnet $Rb_2Mn_cMg_{1-c}F_4$. The concentrations studied are $c=0.54$, $c=0.57$, and $c=0.60$; the site-percolation concentration for the nearest-neighbor square lattice is $c_p=0.593$ so that these experiments span the percolation threshold. The point $c=c_p$, $T=0$ represents the percolation multicritical point which terminates the line of second-order transition of the infinite network. We give a detailed description of the theory of the magnetic behavior around the percolation point; as the temperaturelike scaling field we suggest $\mu(T)=\kappa_1(T)$ where $\kappa_1(T)$ is the inverse correlation length for the associated one-dimensional chain; for the static structure factor we propose the formula $S(|c_p-c|, \mu, \vec{Q}) \propto \kappa^{\eta}(\kappa^2+Q^2)^{-1}$, where $\kappa=\kappa(|c_p-c|, 0)+\kappa(0,\mu)$; that is, we assume that the geometrical and thermal inverse correlation lengths are simply additive. The $c=0.60$ sample is found to have a smeared second-order phase transition at about 8 K to a state with two-dimensional long-range order but only weak correlations in the third direction. The spin fluctuations in the precritical region are essentially identical to those in the concentrated systems, thus demonstrating that the phase transition in the $c=0.60$ infinite network is little affected by the proximity to the percolation threshold. For the $c=0.54$ and $c=0.57$ samples the correlation lengths and susceptibility increase with decreasing temperature down to about 3 K, below which temperature they saturate; for both samples the inverse correlation length is well described by the simple formula $\kappa=\kappa(\Delta C,0)+[\kappa_1(T)]^{0.9\pm0.05}$; the susceptibility follows the law $S(0)\sim\kappa^{1.5\pm0.15}$; both results are consistent with our scaling crossover formula and the assumption of the importance of the underlying one-dimensional links in the percolation clusters. The corresponding thermal critical exponents are $\nu_T=0.9\pm0.1$ and $\gamma_T=1.5\pm0.15$ compared with the percolation exponents $\nu_p=1.36$ and $\gamma_p=2.43$, so that the experimental crossover exponent is $\phi=1.56\pm0.15$. There is currently no first-principle theory which properly accounts for this value of the crossover exponent, although the experiment includes within the errors the value $\phi=1.7$, appropriate to a self-avoiding walk ansatz for the principal paths along which the correlations spread.

## I. INTRODUCTION

In the first of this set of papers[1] (hereafter referred to as I), we reported the results of a detailed study of the spin dynamics in the mixed magnetic-nonmagnetic two-dimensional antiferromagnet $Rb_2Mn_cMg_{1-c}F_4$. The experiments were initiated primarily to elucidate certain controversial issues in theories of the dynamics of highly random systems.[2] The concentrations $c$ were chosen to be near the nearest-neighbor percolation threshold,[3] $c_p$, in order to make as varied as possible the local magnetic-ion configurations while at the same time retaining quite large connected clusters. We had hoped, in addition, that one would be able to study percolation effects in a real crystalline system which was both simple and well characterized. However, it was by no means obvious that any real material would exhibit the clean percolation threshold so easily achieved in idealized computer models.[3,4] As we have briefly discussed previously,[5] a well-defined percolation transition is observed in the two-dimensional (2-D) mixed antiferromagnet $Rb_2Mn_cMg_{1-c}F_4$ for $c\simeq0.593$, the percolation threshold for the nearest-neighbor (nn)

 

square-lattice-site problem. In this paper we report a detailed study of the spin correlations using neutron scattering techniques as a function of temperature and concentration for three concentrations spanning the percolation threshold.

The essential features of percolation effects in magnetic materials may be summarized as follows. As a model percolative system, and indeed the one relevant to our actual material, consider a simple square magnet with only nearest-neighbor exchange. If a small number of magnetic atoms $(1-c)$ are removed, then we expect the phase-transition temperature $T_N(c)$ to decrease linearly with $c$, due to the linear decrease in the effective exchange field. As $c$ is further decreased, the network begins to take on a ramified character, and isolated islands of spins appear. Finally, as $c$ reaches $c_p$, the, percolation threshold, the fraction of spins in the infinite network approaches zero; correspondingly, the phase-transition temperature approaches $T_N(c_p)=0$. Finally, for $c < c_p$ the system consists exclusively of finite clusters, so that there can be no long-range order. The point $c=c_p$, $T=0$ thus represents the termination point of the line of continuous transitions of the infinite network. One may observe *geometrical* critical behavior around $c=c_p$ by varying the concentration $c$ at $T=0$. Alternately one may observe *thermal* critical behavior in the percolation network by fixing $c$ equal to $c_p$ and varying the temperature. The point $c=c_p$, $T=0$ thus represents an especially interesting *multicritical* point involving, in general, both geometrical and thermal critical fluctuations.[6–8] Since our original publication, a number of theories for the behavior around the percolation multicritical point have appeared[7–17]; we shall, therefore, discuss our results in the context of these theories.

Finally, we should note that these theories made especially clear the need for ancillary experiments in a diluted 2-D Ising model. A series of experiments have therefore been performed in the isostructural system $Rb_2Co_cMg_{1-c}F_4$. The Co–Co interactions have a pronounced Ising anisotropy as opposed to the Mn–Mn interactions which are essentially Heisenberg-like in character. The $Rb_2Co_cMg_{1-c}F_4$ results will be described in Paper III of this series.[18] Not surprisingly, the Ising and Heisenberg systems exhibit a number of interesting differences; accordingly we will make detailed comparisons of the two materials both in this paper and in Paper III.

The format of this paper is as follows. In Sec. II we give a brief summary of the properties of the materials together with a discussion of the elements of neutron scattering theory; Sec. III reviews the current picture of magnetic-percolation theory with specific application to $Rb_2Mn_cMg_{1-c}F_4$. In Sec. IV we describe the quasielastic and inelastic neutron scattering measurements. The theoretical analysis and conclusions are given in Sec. V.

## II. PRELIMINARY DETAILS

### A. Crystal and magnetic-structure properties

The crystal and magnetic structure of $Rb_2MnF_4$ and the alloys $Rb_2Mn_cMg_{1-c}F_4$ have been discussed extensively in Paper I; the reader is referred to that paper for full details. In order to facilitate discussion of the explicit scans carried out in these experiments, we show in Fig. 1 the crystal structure together with the (010) magnetic zone of the reciprocal lattice. In Paper I we discussed measurements on two samples of $Rb_2Mn_cMg_{1-c}F_4$, one with $c=0.54\pm0.02$ and a second with $c=0.57\pm0.02$; these concentrations were inferred from the results of a number of measurements including those described in this paper; the absolute concentrations are believed to be accurate to $\pm0.02$ as quoted above.

In this paper we shall describe measurements on the above two samples, together with a third for which the concentration was chosen to be above the 2-D square-lattice percolation threshold[3,19] $c_p=0.593$. The nominal $Mn^{++}$ concentration in this third sample is 61%. The lattice constants measured at 5 K are $a=4.1542$ Å and $c=13.806$ Å. By comparison with the values obtained for the 54% and 57% samples as quoted in Table I of Paper I, we conclude that the actual $Mn^{+++}$ concentration in this sample is $c=0.60\pm0.02$; we should emphasize that the differences are known rather more accurately than the absolute values. In the absence of any clustering effects, we anticipate that for $c > c_p=0.593$ a transition to long-range order will occur at nonzero temperature. As

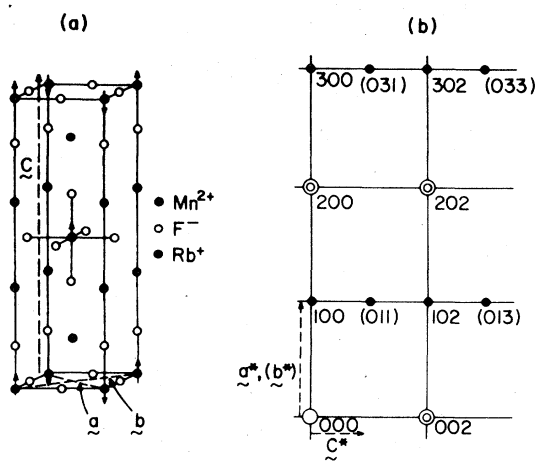


FIG. 1. (a) Crystal and magnetic structures of $Rb_2MnF_4$. Inverting the central spin exchanges the $a$ and $b$ magnetic axes. Here we show only the $K_2NiF_4$-type magnetic structure; the $Ca_2MnO_4$-type structure may be generated by inverting the spins of the nnn layer. (b) (010) and (100) magnetic zones of the reciprocal lattice; again we show only $K_2NiF_4$-type Bragg positions. Nuclear Bragg peaks are indicated by double circles.

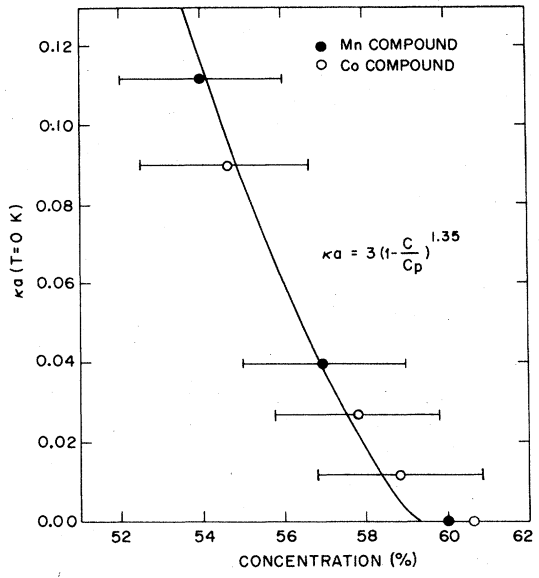


FIG. 2. $T=0$ inverse correlation length vs concentration in $Rb_2Mn_cMg_{1-c}F_4$ and $Rb_2Co_cMg_{1-c}F_4$; the error bars represent the uncertainties from the chemical analysis; the relative concentrations for the Mn and Co compounds separately are known to about 1%; the Mn compound concentrations are discussed in Paper I; the Co compound concentrations are from the chemical analysis.

we shall discuss in Sec. IV, this third sample does indeed order at 8 K. Finally, as outlined in Sec. III, the percolation correlation length at $T=0$ may provide a very accurate measure of the concentration for samples with $c \lesssim c_p$. Unfortunately only the percolation exponent and not the absolute amplitude is known. It is of interest, nevertheless, to plot the inverse correlation lengths observed at low temperatures both for the $Mn^{++}$ compounds and for the isostructural $Co^{++}$ compounds to be discussed in Paper III; these results are shown in Fig. 2; quite gratifyingly all of the results fall on a smooth curve, suggesting that our error limits of $\pm 0.02$ may be too conservative. We shall discuss the theoretical curve in Fig. 2 later in this paper. As discussed in Paper I and as supported by the data presented here, we may take the concentrations to be 0.54, 0.57, and 0.60; henceforth we shall refer to these samples as 54%, 57%, and 60%.

### B. Neutron scattering cross section

If the neutron energy loss in the experiments is $\hbar\omega$ and the wave-vector transfer is $\vec{Q}$, the differential magnetic-scattering cross section for upolarized neutrons may be written[20] for our conditions

$$\frac{d^2\sigma}{d\Omega\, d\omega} = \left(\frac{\gamma e^2}{m_e c^2}\right)^2 \frac{k_1}{k_0} I(\vec{Q},\omega) \ , \tag{1}$$

where

$$I(Q,\omega) = |f(\vec{Q})|^2[(1+\sin^2\theta)S^{\perp}(\vec{Q},\omega) + \cos^2\theta S^{\parallel}(\vec{Q},\omega)] \ , \tag{2}$$

where $k_0$ and $k_1$ are the wave vectors of the incident and scattered neutrons and $f(\vec{Q})$ is the form factor of the Mn ions. The angle $\theta$ is the angle between $\vec{Q}$ and the crystallographic $c$ axis, and the correlation functions are given by

$$S^{\perp}(\vec{Q},\omega) = \frac{1}{2\pi}\int_{-\infty}^{\infty} dt\, e^{-i\omega t} \sum_{mn} e^{i\vec{Q}(\vec{R}_m-\vec{R}_n)} \tfrac{1}{4}\langle S_m^+(t)S_n^-(0) + S_m^-(t)S_n^+(t)\rangle \ , \tag{3}$$

$$S^{\parallel}(\vec{Q},\omega) = \frac{1}{2\pi}\int_{\infty}^{\infty} dt\, e^{-i\omega t} \sum_{mn} e^{i\vec{Q}(\vec{R}_m-\vec{R}_n)} \langle S_m^z(t)S_n^z(0)\rangle \ , \tag{4}$$

where the summations over $m$ and $n$ are over all the magnetic sites at $\vec{R}_m$ and $\vec{R}_n$. The axes for the spin components are chosen to coincide with the crystallographic axes; namely, $z$ is along the (001) $c$ axis, and we have made use of the symmetry of the system. If the only interactions between the spins were of the Heisenberg form, the spin system would have isotropic symmetry and

$$S^{\perp}(\vec{Q},\omega) = S^{\parallel}(\vec{Q},\omega) \ .$$

The integrals of the scattering functions over all frequencies give the total scattering functions

$$S^{\parallel}(\vec{Q}) = \int_{\infty}^{\infty} S^{\parallel}(\vec{Q},\omega)\, d\omega \ , \tag{5}$$

$$S^{\perp}(\vec{Q}) = \int_{-\infty}^{\infty} S^{\perp}(\vec{Q},\omega)\, d\omega \ . \tag{6}$$

The scattering functions may be related to the generalized frequency and wave-vector-dependent magnetic susceptibility, namely,

$$S^{\parallel}(\vec{Q},\omega) = \frac{1}{g^2\mu_B^2}[n(\omega)+1]\,\mathrm{Im}[\chi^{\parallel}(Q,\omega)] \ , \tag{7}$$

where $n(\omega)$ is the Bose-Einstein occupation factor $n(\omega) = [\exp(\hbar\omega/k_BT)-1]^{-1}$, and a similar relation connects $S^{\perp}(\vec{Q},\omega)$ and $\chi^{\perp}(\vec{Q},\omega)$. If $\hbar\omega \ll k_BT$, a Kramers-Kronig relation then provides a relationship between the static susceptibility and the total scattering functions as

$$S^{\perp}(\vec{Q}) = \frac{k_BT}{(g\mu_B)^2}\chi^{\perp}(\vec{Q},0) \tag{8}$$

and

$$S^{\parallel}(\vec{Q}) = \frac{k_B T}{(g\mu_B)^2} \chi^{\parallel}(\vec{Q}, 0) \quad , \tag{9}$$

so that the wave-vector-dependent susceptibility can be deduced directly from measurements of the total scattering.

We note that in Eqs. (3) and (4) the magnetic scattering will, of course, be zero from unoccupied sites, that is $S_{Mg}=0$. Less trivially, but even more importantly, for $c < c_p$ where the system has broken up into finite clusters, we anticipate that the spins in different clusters will be uncorrelated. In that situation, the neutrons will measure the pair correlations within a given cluster and these will then be averaged over all clusters in the material.

## III. MAGNETIC-PERCOLATION PHENOMENA

### A. Percolation theory and neutron scattering

The pure percolation problem has now been discussed by a wide variety of authors. We refer the reader to reviews listed in Ref. 3 and to the recent papers by Reynolds and co-workers.[19–22] We give here only a brief description of the current theoretical picture. As discussed in Sec. I, for illustrative purposes we consider a simple square lattice with bonds between nearest-neighbor sites alone. As sites are removed, initially the network simply becomes diluted. However, gradually finite clusters appear which are isolated from the infinite network. With increasing vacancy concentration these finite clusters grow while the number of sites in the infinite network decreases precipitously. Finally at a well-defined site concentration $c_p$ the infinite network vanishes, and the system is made up exclusively of finite clusters, albeit, at $c_p$, spanning a range from 1 to $\infty$ number of constituent sites. As the site concentration is decreased further below $c_p$, the clusters decrease both in linear extent and in terms of the mean number of sites per cluster. For illustrative purposes we show in Fig. 3 a computer-generated percolation sample for $c=0.50$.

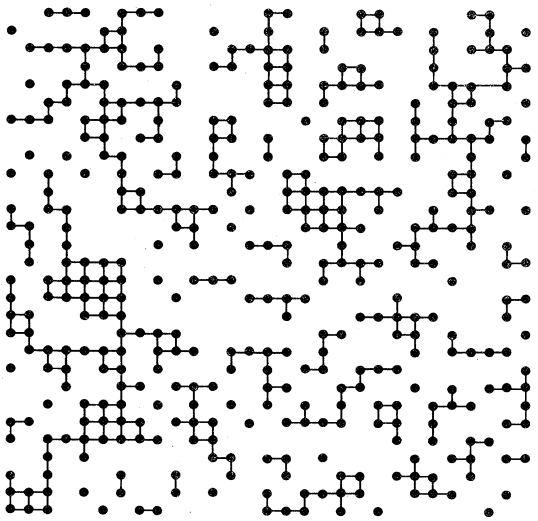

FIG. 3. Computer simulation of the shape of the Mn clusters for a 2-D nn site-random square lattice with $c=0.50$.

In an important paper Kasteleyn and Fortuin[23] showed that the percolation transition may be mapped into a lattice-gas model, specifically the $V \to 1$ limit of the $V$-component Potts model. That is, the point $c=c_p$ represents a *critical point* and the system exhibits *geometrical critical behavior* around $c=c_p$.

It is convenient to define the following quantities which characterize the cluster statistics for a given concentration $c$.[3]

*i. Pair connectedness:* The pair connectedness $C_2(r)$ is the conditional probability that given an occupied site at the origin, a site at a distance $r$ away is occupied and in the same cluster. Our experiments suggest an Ornstein-Zernike form for $C_2(\vec{q})$, the Fourier transform of $C_2(r)$, so that in two dimensions we have

$$C_2(r) \sim \frac{e^{-r/\xi_G}}{r^{1/2}} \quad \text{for } \xi_G < \infty \quad . \tag{10}$$

At $c=c_p$ where $\xi_G=\infty$, Eq. (10) becomes $C_2(r) \sim r^{-\eta}$.

*ii. Geometrical correlation length.* We denote $\xi_G$ in Eq. (10) as the geometrical correlation length.

*iii. Mean number of finite clusters of any size.* The mean number of clusters, normalized per site, of a given size $s$ is $\langle n_s \rangle$; then the mean number of clusters of any size is

$$G(c) = \sum_s^f \langle n_s \rangle \quad ,$$

where the superscript "f" on the sum denotes the exclusion of the infinite cluster, if one exists.

*iv. Fraction of occupied sites that belong to the infinite cluster.* This fraction is defined by

$$P(c) = 1 - \left( \sum_s^f s \langle n_s \rangle / \sum_s s \langle n_s \rangle \right) \quad . \tag{11}$$

*v. Mean size of the finite clusters.* This is defined in terms of the quantities defined above as,

$$S(c) = \left( \sum_s^f s^2 \langle n_s \rangle / \sum_s^f s \langle n_s \rangle \right) \quad . \tag{12}$$

The following correspondences exist between these functions and the thermodynamic functions of a magnet: Pair connectedness $C_2(r) \leftrightarrow$ pair-correlation

function; geometrical-correlation length $\xi_G \leftrightarrow$ thermal-correlation length; mean number of clusters $G(c) \leftrightarrow$ free energy; percolation probability $P(c) \leftrightarrow$ magnetization; mean size of finite clusters $S(c) \leftrightarrow$ zero-field susceptibility. Not surprisingly, there is also a direct analogue of the static variant of the fluctuation-dissipation theorem; it may be simply written[21]

$$\int \vec{d}r C_2(\vec{r}) = S(c) \ . \tag{13}$$

Now let us address the issue of how one may measure $S(c)$, $P(c)$, and $C_2(r)$ in a real material. We consider first the neutron scattering from the nuclei of a binary alloy. As is well known,[20] for a purely random uncorrelated two-component system with scattering lengths $b_1$ and $b_2$ and concentrations $c_1 = c$ and $c_2 = 1 - c$, the cluster scattering cross section contains a coherent nuclear Bragg term $\bar{b}^2 \delta(\vec{Q} - \vec{\tau})$ together with a spatially uniform incoherent cross section proportional to $b^2 - \bar{b}^2$; here $\bar{b} = c_1 b_1 + c_2 b_2$ and $b^2 = c_1 b_1^2 + c_2 b_2^2$. Thus the elastic neutron scattering cross section contains no information at all about the cluster statistics. The essential reason for this is, of course, that all atoms in the crystal contribute equally to the total scattering; that is, there is no mechanism differentiating the scattering within one cluster from the between-cluster terms. Conversely, it is clear that, in order to observe $C_2(r)$, one requires a mechanism which will cause atoms within a given cluster to scatter coherently but will simultaneously produce incoherent scattering between different finite clusters. It is clear that this situation may be realized if the percolative species is magnetic; further, we require that the appropriate range of interaction used to define the cluster statistics be just the range of the magnetic interaction.

The situation is most easily envisaged for a nearest-neighbor Ising ferromagnet.[24] At $T = 0$ the spins within a cluster will all be parallel; however, the net spin of the cluster will be randomly up or down. Then, by definition, in the longitudinal structure factor

$$S^{\parallel}(\vec{Q}) = \sum_{m,n} e^{i\vec{Q}\cdot(\vec{R}_m - \vec{R}_n)} \langle S_m^z(0) S_n^z(0) \rangle_T \ , \tag{14}$$

the two-spin correlation function $\langle S_m^z(0) S_n^z(0) \rangle_{T=0}$ will equal $S^2$ if $m$ and $n$ belong to the same cluster and will equal zero otherwise. It is evident that $S(Q = 0)$ will be simply proportional to $S(c)$, the mean size of the finite clusters in the percolation problem and that, more generally, $S^{\parallel}(\vec{Q})$ is simply proportional to the Fourier transform of the percolation pair connectedness $C_2(r)$, since $S_n^z(0) = 0$ if $n$ is unoccupied. Finally, for $c > c_p$, the magnetic Bragg-peak intensity will be simply proportional to $P^2(c)$, the square of the fraction of atoms belonging to the infinite network. For an antiferromagnet similar results hold for $S(\vec{q}^*)$ where $\vec{q}^*$ is an antiferromagnetic reciprocal-lattice position.

### B. Magnetism near the percolation threshold

We have already discussed this briefly in the Introduction; we note that, since our original publication on part of this work, a large number of theories[7–17] together with some new experiments[25] have appeared; it is therefore now possible to give a more cohesive discussion. We begin at the $c = 1$ limit. With initial removal of $(1 - c)$ atoms we expect simply that the phase-transition temperature will decrease linearly with $1 - c$, that is

$$T_N(c)/T_N(1) = 1 - \alpha(1 - c) + \cdots \ . \tag{15}$$

In mean-field theory, one expects $\alpha = 1$. In fact, however, for the 2-D square-lattice random-bond nearest-neighbor Ising model one finds[12,26] $\alpha = 1.329$. The critical behavior for $c < 1$ will be that of the appropriate random 2-D system; as we shall discuss below, in $Rb_2Mn_cMg_{1-c}F_4$ and its isomorphs there is a small Ising anisotropy so that the critical behavior is that of the 2-D random Ising model — experimentally,[27] this turns out to be indistinguishable from that of the normal 2-D Ising model with critical exponents: order parameter $\beta = 0.125$, longitudinal susceptibility $\gamma = 1.75$, longitudinal correlation length $\nu = 1$ and, in accordance with scaling, $\eta = 2 - \gamma/\nu = 0.25$.

As $c$ is further decreased towards the percolation threshold, the number of spins in the infinite network decreases precipitously. Accordingly, $T_N(c)$ decreases rapidly; finally for $c < c_p$ there is no infinite network, so that there can be no phase transition to long-range order (LRO); concomitantly $T_N(c_p) = 0$; we shall, of course, be especially interested in the manner in which $T_N(c)$ approaches zero. The general behavior is shown schematically in Fig. 4. We shall discuss the differences between the Ising, Heisenberg-Ising, and Heisenberg models below. It is clear that one has a line of critical points which terminates at the point $c = c_p$, $T = 0$. This special point in the $T$, $c$ phase diagram is termed the percolation multicritical point.[6–8] That the percolation point in magnets can be viewed as a multicritical point was originally presented as an ansatz by Stauffer,[6] and elaborated by Stanley *et al.*[7] and Lubensky.[8] More recent theories[9–17] have substantiated this hypothesis. In essence, this means that the percolation point may be approached along two essentially different directions — the concentration axis with $T = 0$ and the temperature axis with $c = c_p$. For very low temperatures we expect pure *geometrical* critical behavior.

Recent theories for the appropriate exponents in two dimensions[19,22] give

$$\begin{aligned} &\xi_G \sim |c_p - c|^{-\nu_p}, \quad \nu_p = 1.355 \pm 0.015 \ , \\ &S(c) \sim |c_p - c|^{-\gamma_p}, \quad \gamma_p = 2.425 \pm 0.0005 \ , \\ &P(c) \sim (c - c_p)^{\beta_p}, \quad \beta_p = 0.139 \pm 0.005 \ , \end{aligned} \tag{16}$$

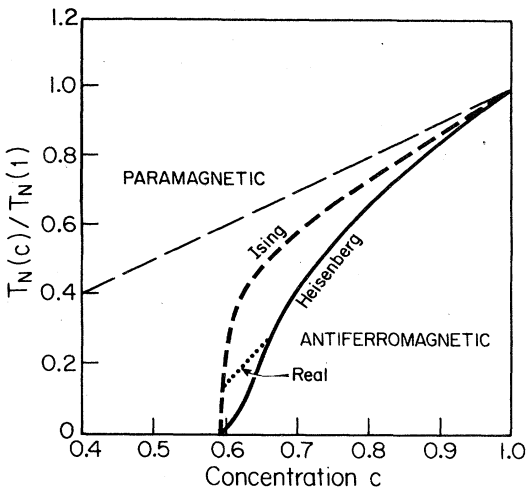


FIG. 4. Schematic phase diagram of a diluted 2-D square-lattice antiferromagnet with nearest-neighbor interactions. The Heisenberg system is assumed to have an infinitessimal 3-D interaction in order to produce a phase transition to conventional long-range order. The "real" curve corresponds to a 2-D Heisenberg model with about 1% dipolar Ising anisotropy.

and finally $n_p = 2 - \gamma_p/\nu_p = 0.20 \pm 0.01$.

In order to discuss the *thermal* critical behavior it is first necessary to choose the appropriate temperaturelike scaling field. Near a normal finite-temperature phase transition for $T \simeq T_c$ this usually reduces simply to the reduced temperature difference $|\tau| = |1 - T/T_c|$. However, for a system with $T_c = 0$ K the problem is more complicated. In a previous publication[5] we made the following heuristic argument. From Fig. 3, it is evident that typical clusters have a highly ramified character and, in particular, for the spin correlations to extend over any distance, they must propagate through many *one-dimensional paths.* These 1-D chains should represent the controlling factor since they are most susceptible to thermal fluctuations. Thus the appropriate temperature variable is plausibly taken as the *one-dimensional inverse correlation length* $\kappa_1(T)$ for a linear chain with the equivalent Hamiltonian. Similar arguments have been given by Stauffer,[6] Stanley *et al.*,[7] and Lubensky.[8] In the Ising and Heisenberg limits $\kappa_1(T)$ reduces to (Ising)

$$\kappa_1(T) = \ln[\tanh(J/kT)] \simeq 2e^{-2J/kT}, \tag{17}$$

(Heisenberg)

$$\kappa_1(T) = \ln(\coth J/kT - kT/J) \simeq kT/J, \tag{18}$$

where $J$ is the pair energy for parallel spins for classical unit-length spins. In many real Heisenberg-like systems, there is also a small dipolar Ising-anisotropy term. As we have discussed previously,[5,25] an Ising perturbation $H_A$ will cause a crossover in $\kappa_1^{\parallel}(T)$ from linear to exponential behavior in temperature for $kT < (J \cdot H_A)^{1/2}$. Here the $\parallel$ superscript implies the component along the anisotropy axis. As we shall see, this spin-space crossover does indeed manifest itself in a dramatic fashion in our experiment. In this paper, therefore, we shall take as the temperature scaling field $\mu(T) = \kappa_1^{\parallel}(T)$, where $\kappa_1^{\parallel}(T)$ should ideally be calculated exactly. We should note that other authors have also used Eqs. (17) and (18) for the Ising and Heisenberg limits. So far, however, our more general ansatz of $\mu(T) = \kappa_1^{\parallel}(T)$ represents the only technique, heuristic or otherwise, for including spin-space-crossover effects which are, of course, important in most real systems.

Having argued that $(c_p - c)$ and $\mu(T) = \kappa_1^{\parallel}(T)$ are the appropriate variables, one may now give a standard multicritical scaling description. Here we give only a few essential results, and the reader is referred to Ref. 7 for a full description. (i) For $\mu = 0$, one will obtain pure percolation critical behavior with critical exponents $\nu_p$, $\gamma_p$, $\eta_p$ for the fluctuations. (ii) For $c = c_p$ one will obtain pure thermal critical behavior with exponents $\nu_T = \nu_p/\phi$, $\gamma_T = \gamma_p/\phi$, and $\eta_T = \eta_p$. Here $\phi$ is the percolation-crossover exponent. (iii) For $c > c_p$ the line of second-order transitions will approach the $\mu = 0$ axis along the path $\mu(T_c) \sim (c - c_p)^{\phi}$. (iv) For $c < c_p$ one will observe a crossover from thermal to geometrical critical behavior at a reduced temperature $\mu^x(T) \sim (c_p - c)^{\phi}$; physically, this simply means that the correlations will grow until they equal the size of the clusters, and this will be achieved at $\mu \sim \mu^x(T)$.

So far most theoretical attention has been directed towards the crossover exponent $\phi$ itself. As we shall discuss below, for $d = 1$ the problem is exactly soluble,[28] and one finds $\phi = 1$. For $d > 6$, mean-field theory is correct,[29,30] and one again has $\phi = 1$. For $1 < d < 6$ it is now believed[10] that for the Ising model $\phi = 1$ always; thus for Ising systems in any dimension, the theory predicts that all paths leading to $c = c_p$, $\mu = 0$ will be described by a single set of critical exponents; these will, of course, be just those characteristic of the pure percolation problem. Further, the second-order phase-transition line should then approach the percolation point linearly in $c - c_p$; that is, for an Ising system one expects $e^{-2J/kT_c} \sim c - c_p$. For the Heisenberg or near-Heisenberg systems the theory is on much less firm a foundation. Stanley *et al.*,[7] following a suggestion of Anderson[31] have developed a theory which takes as an ansatz that the magnetic correlations spread through the incipient infinite cluster for $c \sim c_p$ along a path that is a self-avoiding walk.[32] In two dimensions this theory predicts[7] $\phi = 1.7$. Other theories predict $\phi$ values closer to unity and, indeed, Stinchcombe[16] has suggested that the Heisenberg result is probably identical to the Ising result, $\phi = 1$.

For the purposes of analyzing our neutron scattering data, the above theory is incomplete. In particular, one would ideally like a closed-form analytic expression for the structure factor $S(\Delta c, \mu, \vec{Q})$. This requires an explicit calculation of the crossover function and not just the exponent $\phi$. No such theory is yet available. Fortunately, however, the problem is exactly soluble in one dimension for classical spins, and this case provides some useful guidance.[28] In one dimension the percolation point is simply $c_p = 1$, since a single vacancy will break a linear chain into two. Thorpe's exact solution for the 1-D problem may be written in the form

$$S(\Delta c, \mu, \vec{Q}) \propto \frac{\kappa(\Delta c, 0) + \kappa(0, \mu)}{[\kappa(\Delta c, 0) + \kappa(0, \mu)]^2 + Q^2} + O[(\Delta c)^2, \mu^2] \ , \tag{19}$$

where $\kappa(\Delta c, 0) = 1 - c$, and $\kappa(0, \mu) = \mu = \kappa_1^{\parallel}(T)$ by definition. It is apparent from Eq. (19) that $\phi = 1$ in one dimension. Equation (19) may be generalized to $d$ dimensions in a number of ways; the simplest of these we might postulate is

$$S(\Delta c, \mu, \vec{Q}) = \frac{A \kappa^{\eta}}{\kappa^2 + Q^2} \ , \tag{20}$$

with

$$\kappa = \kappa(\Delta c, 0) + \kappa(0, \mu)$$

and

$$\kappa(\Delta c, 0) \sim (\Delta c)^{\nu_p}, \kappa(0, \mu) \sim \mu^{\nu_p/\phi} \ .$$

This assumes that the crossover enters in the simplest fashion possible. As we shall see, Eq. (20) is quite successful in representing our experimental data both in $Rb_2Mn_cMg_{1-c}F_4$ and $Rb_2Co_cMg_{1-c}F_4$. Clearly, however, a more rigorous theory is desirable.

### C. Application to $Rb_2Mn_cMg_{1-c}F_4$

As discussed extensively in Paper I, the $Mn^{++}$ spins form a simple square lattice with Hamiltonian

$$\mathcal{H} = \sum_{\langle nn \rangle} J_{nn} \vec{S}_i \cdot \vec{S}_j + \sum_{\langle nnn \rangle} J_{nnn} \vec{S}_i \cdot \vec{S}_j - g \mu_B H_A \sum_i (-)^i S_i^z \ , \tag{21}$$

where all the sites on one magnetic sublattice have $i$ even and others have $i$ odd and the summations are over nearest-neighbor and next-nearest-neighbor pairs. In pure $Rb_2MnF_4$, $J_{nn} = 0.653$ meV, $J_{nnn} = 0.012$ meV, and $g\mu_B H_a = 0.031$ meV. More distant-neighbor interactions appear to be negligible. In the diluted system $Rb_2Mn_{0.54}Mg_{0.46}F_4$, $J_{nn}$ increases to 0.72 meV due to the decrease in lattice constant.[1] We shall use this latter value in this paper. The interactions are thus overwhelmingly between nearest neighbors alone.

We note that the nnn interaction is very much weaker. Hence, we expect $Rb_2Mn_cMg_{1-c}F_4$ to be a good realization of the near-Heisenberg 2-D nn site random percolation magnet.

Let us now discuss the role played by the anisotropy term. In two dimensions the anisotropy plays an essential role since it lifts the pathology associated with the 2-D Heisenberg model.[33] Indeed, as has been extensively documented experimentally,[27] $Rb_2MnF_4$ exhibits a 2-D Ising-like phase transition in spite of the fact that the anisotropy field is less than 0.5% of the isotropic exchange field. The phase-transition temperature itself, however, corresponds closely to that estimated by Stanley and Kaplan[33] from high-temperature-series expansions for the pure Heisenberg system; that is, the anisotropy field permits a phase transition to a conventional long-range-ordered state, but the magnitude of $T_c$ depends only weakly on $H_A$. We shall assume that similar behavior results for the diluted samples for $c$ not too close to $c_p$.

As we have discussed in Sec. III B, the anisotropy plays an essential role near $c_p$ for spin systems of all dimensions, not just two. This may be illustrated directly for $Rb_2Mn_cMg_{1-c}F_4$. We have suggested on a heuristic basis that one should use $\kappa_1^{\parallel}(T)$ as the appropriate temperature scaling field. In order to estimate $\kappa_1^{\parallel}(T)$, we have used the results of Blume *et al.*[34] for the classical 1-D Heisenberg magnet in a field. Their classical-spin Hamiltonian is given by

$$\mathcal{H} = \mathcal{J} \sum_{m=1}^{n} \vec{\zeta}_m \cdot \vec{\zeta}_{m+1} - D \sum_{m=1}^{n} (\zeta_m^z)^2 \ , \tag{22}$$

where $\vec{\zeta}$ is a classical unit-spin vector. We have then taken

$$\mathcal{J} = J_{nn} S(S+1) = 73 \text{ K} \ ,$$

$$D = g \mu_B H_A S c \sim 0.53 \text{ K} \ ,$$

so that $D/\mathcal{J} = 0.0073$. The results for the longitudinal and transverse 1-D correlation lengths $\kappa_1^{\parallel}(T)$ and $\kappa^{\perp}(T)$, respectively, so obtained are shown in Fig. 5 together with the corresponding results for the pure Heisenberg and Ising models. It is evident that one expects Heisenberg-like behavior in $Rb_2Mn_{c_p}Mg_{1-c_p}F_4$ down to about 5 K. Below 5 K a crossover to Ising-like behavior is predicted. We should note that in $Mn_cZn_{1-c}F_2$, where we have performed both experiments and similar calculations,[25] this procedure provides a useful semiquantitative guide, but it underestimates the crossover temperature by about a factor of 2, presumably due to quantum effects. We might expect a similar underestimate in $Rb_2Mn_cMg_{1-c}F_4$.

Finally, we should note that the above calculations

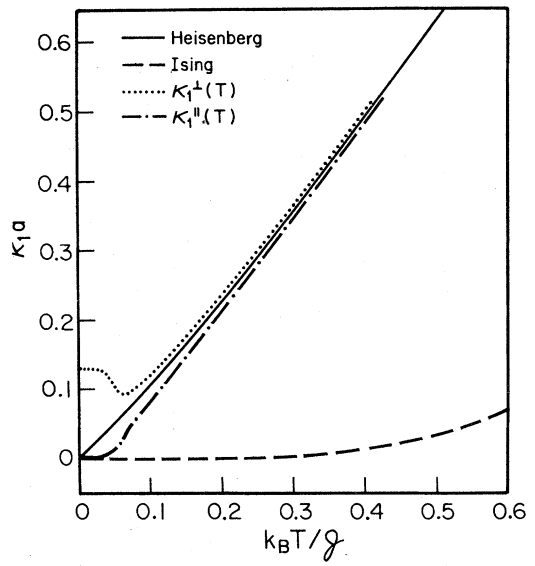


FIG. 5. One-dimensional inverse correlation lengths for a unit-vector classical-spin model with Ising, Heisenberg, and Heisenberg plus 0.73% anisotropy field symmetries. The curves labeled $\kappa_1^{\parallel}$ and $\kappa_1^{\perp}$ correspond to the final model; $\parallel$ and $\perp$ are defined relative to the anisotropy axis.

provide an immediate explanation of the phase diagram for $K_2Mn_cMg_{1-c}F_4$ (and correspondingly $Rb_2Mn_cMg_{1-c}F_4$) as measured by Breed *et al.*[35] and as illustrated qualitatively in Fig. 4 by the curve labeled "Real". From the scaling theory $\mu(T_c) \sim (c - c_p)^{\phi}$ with $\phi$ at least close to 1. Hence the $T_c$ vs $c - c_p$ phase diagram should show an initial, very rapid, logarithmic dependence of $T_c$ on $\Delta c$ followed by a much more gradual increase. Such behavior is indeed observed, thus giving direct support to our theoretical approach.

We now discuss the experimental results.

## IV. EXPERIMENTAL RESULTS

### A. $c = 0.60$

We discuss first the experiments on the sample with $c = 0.60 > c_p = 0.593$. The experiments were performed on a two-axis spectrometer at the Brookhaven High Flux Beam Reactor. The incident neutron energy in these experiments was primarily either 13.7 or 5 meV. In all cases the horizontal collimators were 10 min throughout the spectrometer. Either pyrolytic graphite (13.7 meV) or cooled beryllium (5 meV) was used to eliminate higher-order neutrons reflected by the monochromator. We discuss here mainly the measurements carried out at 13.7 meV. For this configuration the dimensions of the resolution ellipsoid were 0.0097 $Å^{-1}$ along the momentum transfer $\vec{Q}$, 0.0020 $Å^{-1}$ perpendicular to $\vec{Q}$ in the scattering plane and 0.082 $Å^{-1}$ vertically, full width at half maximum (FWHM).

Since $c > c_p$, we anticipated that this sample would exhibit a phase transition to antiferromagnetic long-range order at some finite temperature. It should be noted that even for $c - c_p = 0.60 - 0.593 = 0.007$, fully 80% of the atoms belong to the infinite network.[36] Before discussing the explicit scans carried out here, we remind the reader of the analogous results obtained in $Rb_2MnF_4$.

Above $T_N = 38.4$ K, $Rb_2MnF_4$ exhibits pronounced 2-D magnetic short-range-order effects in which near neighbors are antiferromagnetically aligned.[37] This short-range order manifests itself as lines of diffuse magnetic scattering in the (010) zone extending in the $l$ direction along $[h0l]$, centered about $h = 1, 3, \ldots$. At $T_N = 38.4$ K the system undergoes a rather unusual phase transition to 3-D magnetic order. In the same crystal, Birgeneau *et al.*[37] observe two distinct 3-D ordering patterns. In the first, which is illustrated in Fig. 1, the central spin on the near-neighbor (nn) plane may point either up or down, while the spins along the $c$ axis of next-nearest-neighbor (nnn) planes are parallel. This gives rise to the magnetic superlattice peaks shown in Fig. 1(b). This magnetic structure is commonly denoted as the $K_2NiF_4$ structure. However, a second structure also occurs in which the spins of nnn planes along the $c$ axis are antiparallel (the so-called $Ca_2MnO_4$ structure[38]). This gives rise to superlattice scattering at $(h,k,\frac{1}{2}l)$ with $h + k$, $l$ odd. These two structures otherwise have identical magnetic properties, thereby showing that the magnetism is determined largely by the 2-D in-plane interactions.

In order to probe the fluctuations and the possible magnetic ordering in $Rb_2Mn_{0.60}Mg_{0.40}F_4$, we carried out a series of scans along $(1,0,l)$ and across the $(h = 1, 0, l)$ line for various $l$ as a function of $h$. We show in Figs. 6 and 7 the results of a number of such scans. For $T \gtrsim 10$ K the scattering is described by an essentially ideal 2-D Lorentzian profile characteristic of a 2-D fluctuating state.

Explicitly, for $T \geq 10$ K the magnetic scattering is independent of $l$, the coordinate perpendicular to the planes; this, in turn, necessitates that the magnetic correlations are purely 2-D. The in-plane scans across this ridge of scattering correspond to simple Lorentzians with widths significantly larger than the resolution. As the temperature is lowered to 8 K, a rather unusual phase transition is observed. First, as shown in Fig. 6, the scan along the top of the ridge at 8 K is no longer independent of $l$; this in turn means that the spins are now three-dimensionally correlated. As the temperature is further lowered to 1.7 K the peaks at (1,0,0) and $(1,0,\frac{1}{2})$ sharpen somewhat, but they are always much broader than the resolution width. We show in Fig. 7 scans at 9.5 and 6 K across

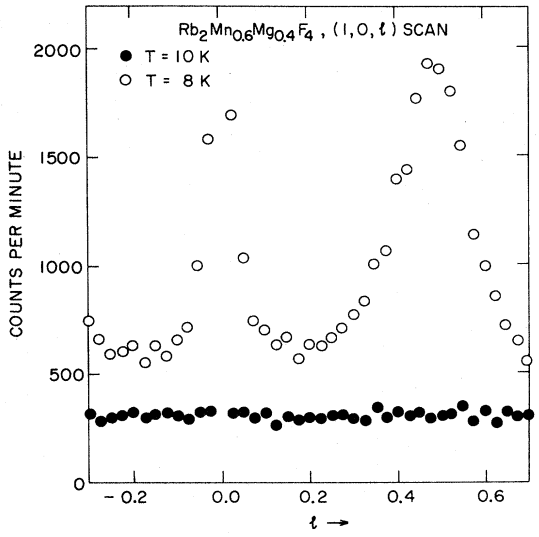


FIG. 6. Scans along $(1,0,l)$ in $Rb_2Mn_{0.60}Mg_{0.40}F_4$.

the ridge at $l=0.2$, which is a minimum intensity position on the ridge. It is evident that at 9.5 K, the scan may no longer be described as a single Lorentzian but instead appears to be the sum of a broad Lorentzian plus a resolution-limited peak at the center. At 6 K one observes a Gaussian profile with a width which is essentially that of the spectrometer resolution function. As the temperature is further lowered to 1.7 K the peak intensity grows somewhat and the background scattering decreases to about eight counts per minute.

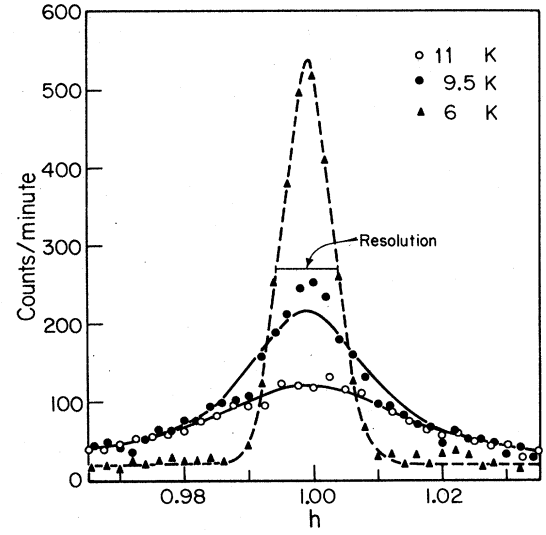


FIG. 7. Results of scans along $[h,0,0.2]$ in $Rb_2Mn_{0.60}Mg_{0.40}F_4$ at the indicated temperatures. The solid lines are the results of fits to a 2-D Lorentzian as described in the text. The dashed line is a guide to the eye. The horizontal bar gives the instrumental FWHM width.

From these scans one may conclude that our sample of $Rb_2Mn_{0.60}Mg_{0.40}F_4$ exhibits a smeared phase transition to 2-D LRO in the temperature range of 7.5 to 9.5 K. As we have noted in Sec. III C, in this concentration range $T_N$ depends logarithmically on $c=c-c_p$, so that only a very slight concentration inhomogeneity will account for the observed smearing. The 3-D aspects of this ordering are, however, rather unusual. In the pure system[37] one observes 3-D resolution-limited peaks at (1,0,0) and $(1,0,\frac{1}{2})$.

In this case the peaks are resolution limited in the $(h,0,0)$ and $(h,0,\frac{1}{2})$ directions, thus confirming the 2-D LRO. However, the FWHM widths in the $l$ direction are approximately 0.08 $c^*$ and 0.18 $c^*$ for $(h,0,0)$ and $(h,0,\frac{1}{2})$. These correspond to between-plane correlation lengths of $\sim 55$ Å and 24 Å, respectively, for the two different ordering configurations. Such unusual behavior has recently been observed in a number of randomized quasi-2-D system.[39] Indeed these systems represent the few cases where randomness has been shown unambiguously to prevent the attainment of full LRO in a 3-D system. In this case, however, the between-plane interaction is $\sim 10^{-6}$ to $10^{-8}$ of $J_{nn}$ so that such severe effects are not surprising.

We have also carried out a series of scans across the ridge as a function of temperature above 10 K in order to characterize the precritical behavior of $\chi(\vec{Q})$. The scans were carried out along $(h,0,0.2)$. At this position the quantity measured is then proportional to

$$I(\vec{Q})=|f(Q)|^2\tfrac{1}{2}[0.988\mathcal{S}^{\parallel}(\vec{Q})+1.012\mathcal{S}^{\perp}(\vec{Q})] \ . \quad (23)$$

As discussed extensively in Ref. 33, in this region of $Q$ space, the inelasticity is taken up completely by the component of the neutron momentum transfer perpendicular to the planes; thus in integrating over the energy, $Q_{2-D}$ is held constant so that the quasi-elastic approximation is essentially exact. Unfortunately, in other regions of $Q$ space where one measures a different combination of $\mathcal{S}^{\parallel}$ and $\mathcal{S}^{\perp}$, this integration may not be performed properly. Hence, only the combination $\mathcal{S}^{\parallel}+\mathcal{S}^{\perp}$ may be obtained with any confidence. Previous experiments[27,33] in the pure systems and in $Rb_2Mn_{0.5}Ni_{0.5}F_4$ have shown that near $T_N$ the magnetic dipole anisotropy plays an essential role and that only $\mathcal{S}^{\parallel}(\vec{q}^*)$ diverges. However, further from $T_c$ we expect that the fluctuations will be approximately isotropic so that the anisotropy will not drastically affect the measured combination of $\mathcal{S}^{\parallel}(\vec{Q})$ and $\mathcal{S}^{\perp}(\vec{Q})$.

The experimental results between 10 and 20 K are quite similar to those shown in Fig. 6 for $T=11$ K. We have fitted the measured profiles to a single Lorentzian

$$I(h,0,0.2)=|f(Q)|^2\frac{a}{\kappa^2+q^2} \ , \quad (24)$$

convolved with the instrumental resolution function; here $\vec{q}=\vec{Q}-\vec{q}^{*}$ is the distance in wave-vector space of the momentum from the nearest 2-D magnetic reciprocal-lattice line and $q^2=q_x^2+q_y^2$. In general, the goodness-of-fit parameter $\chi^2$ varies between 1 and 1.4 thus demonstrating that Eq. (24) adequately describes the experimental data. The inverse correlation length and the peak intensity are shown as functions of temperature in Figs. 8 and 9. In general, the results correspond closely to one's simplest expectations. The data for $\kappa$ fall on an approximate straight line with an extrapolated phase-transition temperature of $\sim 8$ K; this lies within the rounded-phase-transition region of 7.5 to 9.5 K deduced from the 3-D scans. As shown in Fig. 9, the peak intensity varies as $\kappa^{-1.66}$. From Eq. (8) we note that for classical spins $S(0)\sim\chi(\vec{Q})T$. If one plots $S(0)/T$, one finds that, to within the errors, $\chi(0)\sim\kappa^{-2}$, although the exponent 2 is only known to about $\pm 0.3$. In critical exponent language these results correspond to $\nu\sim 1, \gamma\sim 2$ although, of course, the data definitely do not extend into the true critical regime. An experiment covering the same reduced temperature range as these measurements was performed by Als-Nielsen *et al.*[40] in the 2-D alloy $Rb_2Mn_{0.5}Ni_{0.5}F_4$, which has a conventional phase transition at 63.7 K. In this material percolation effects play no role. Als-Nielsen *et al.*[40] also showed that $Rb_2Mn_{0.5}Ni_{0.5}F_4$ exhibits behavior indentical to that of the pure materials $K_2MnF_4$ and $K_2NiF_4$ in the reduced-temperature region where the data overlap. A comparison of our data for $Rb_2Mn_{0.60}Mg_{0.40}F_4$ with the $Rb_2Mn_{0.5}Ni_{0.5}F_4$ experiments shows that the results are essentially equivalent — given, of course, the limitations of our results. Clearly our experiments in $Rb_2Mn_{0.60}Mg_{0.40}F_4$ do not represent an investigation of the true critical behavior; indeed that is not possible in this sample, given the observed smearing of $T_N$. Nevertheless, we may conclude that *the 2-D phase transition is not fundamentally altered despite its close proximity to the 2-D percolation threshold.* This result is consistent with the theory given in Sec. II B.

We now discuss the experimental results in the $c=0.54$ and 0.57 samples.

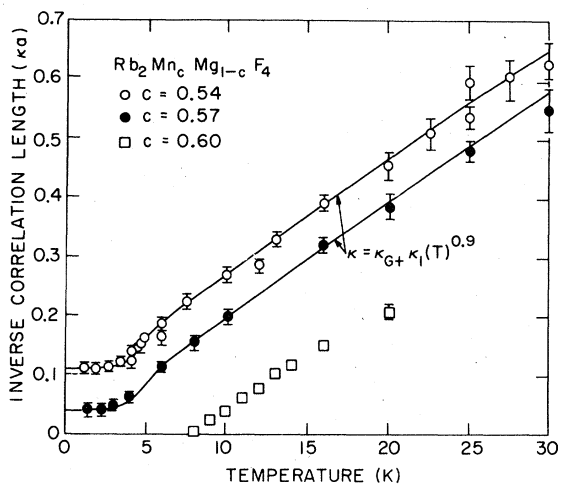


FIG. 8. Fitted inverse correlation lengths vs temperature in $Rb_2Mn_cMg_{1-c}F_4$ for $c=0.54$, 0.57, and 0.60. The solid lines represent fits to the percolation multicritical theory as described in text.

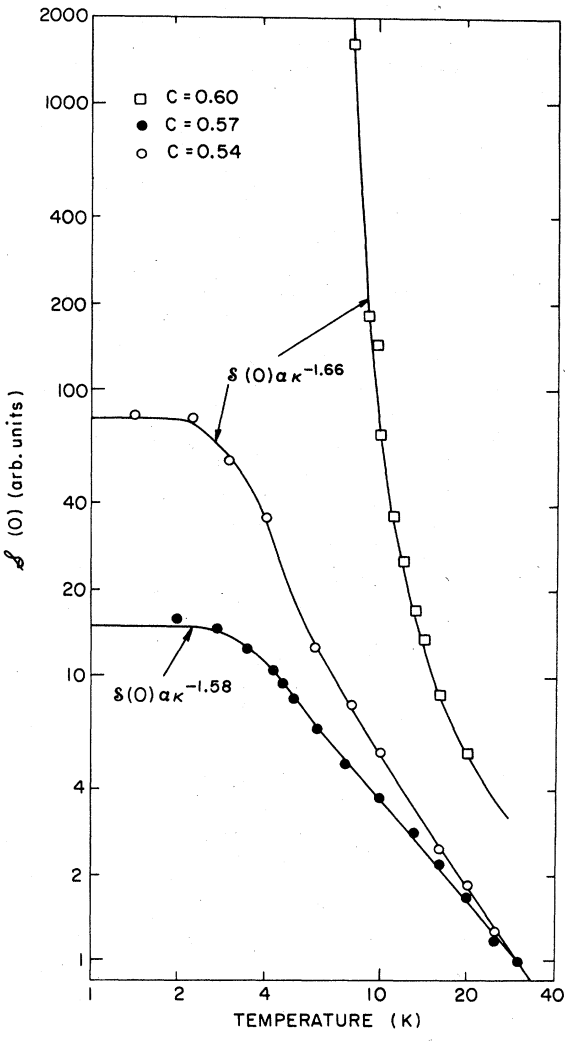


FIG. 9. 2-D magnetic-ridge-peak intensity vs temperature in $Rb_2Mn_cMg_{1-c}F_4$ for $c=0.54$, 0.57, and 0.60. The intensities are on an arbitrary scale. The $c=0.54$ and 0.57 data are normalized at $T=30$ K. For the $c=0.60$ data we have normalized the amplitude $A$ in $S(0)\simeq A\kappa^{-1.66}$ to the value found in the $c=0.57$ sample. The solid lines represent the results of fits to $S(0)\sim\kappa^{-(2-\eta)}$ with the $\kappa$ measured experimentally.

### B. $c = 0.54$ and $c = 0.57$

#### *1. Measurements of the total scattering*

These experiments were carried out in a fashion essentially indentical to that described for the $c = 0.60$ sample. The incident neutron energy was 14.8 meV while the collimator configuration was 20–10–10 min. The resolution ellipse for this configuration was (FWHM) 0.011 $\text{Å}^{-1}$ along $\vec{Q}$, 0.0023 $\text{Å}^{-1}$ perpendicular to $\vec{Q}$ in the scattering plane, and 0.116 $\text{Å}^{-1}$ vertically.

A series of scans was carried out across the ridge along $(h, 0, 0.4)$ and along the top of the ridge $(1, 0, l)$ to probe any possible three dimensionality. Scans were also carried out across the $h = 3$ and $h = 5$ ridges to confirm the basic nn antiferromagnetic nature of the correlations. The essential result is that, for both the 54% and 57% samples, the magnetic scattering takes the form of ridges peaking at $h = 1.0$, 3.0, etc., independent of $l$ except for the magnetic form factor and geometrical factors. As noted in Sec. IV A this is just the form taken by the critical scattering above $T_N$ in the pure systems $K_2MnF_4$ and $K_2NiF_4$ as well as in our $c = 0.60$ sample. We show in Fig. 10 a series of scans across the ridge at $(h, 0, 0.4)$ for various temperatures, in the 54% sample. These data differ in an essential fashion from those shown in Fig. 6 for the 60% sample. The intensity of the scattering increases with decreasing temperature, saturating at a maximum at about 3 K. Correspondingly, the width of the scattering observed in the scans across the ridge decreases with decreasing temperature reaching a constant for $T \leq 3$ K. However, this limiting width is much larger than the spectrometer resolution width in both the 54% and 57% samples. Further, the explicit profile at 3 K and below is Lorentzian rather than Gaussian in character. It is evident, therefore, that we are indeed observing percolation behavior as anticipated in Sec. III.

In order to discuss these data quantitatively, it is necessary to carry out explicit deconvolutions of the data to extract the intrinsic fluctuation parameters. The intensity at $(h, 0, 0.4)$ is given by

$$I(\vec{Q}) = |f(\vec{Q})|^2 [0.95 \mathcal{S}^{\parallel}(\vec{Q}) + 0.05 \mathcal{S}^{\perp}(\vec{Q})] \ . \quad (25)$$

In general, therefore, one expects the measured profiles to be the sum of two Lorentzians originating from the longitudinal and transverse fluctuations. Indeed, in the pure materials[27] near $T_N$, one may clearly separate $\mathcal{S}^{\parallel}$ and $\mathcal{S}^{\perp}$, as we noted previously; for $T >> T_N$, the system becomes essentially isotropic in character so that $\mathcal{S}^{\parallel} \simeq \mathcal{S}^{\perp}$ and one observes a single Lorentzian profile. As discussed in Sec. III C, we may assess the probable importance of the dipolar anisotropy from the calculated behavior of the underlying 1-D correlation lengths as shown in Fig. 5. Recall that for $Rb_2Mn_{0.54}Mg_{0.46}F_4$ one has $\mathcal{J} = 73$ K. From Fig. 5 we judge that for $T > 7$ K the fluctuations will be nearly isotropic, so that Eq. (25) may be well approximated by a single Lorentzian. However, this approximation will undoubtedly break down at the lowest temperatures.

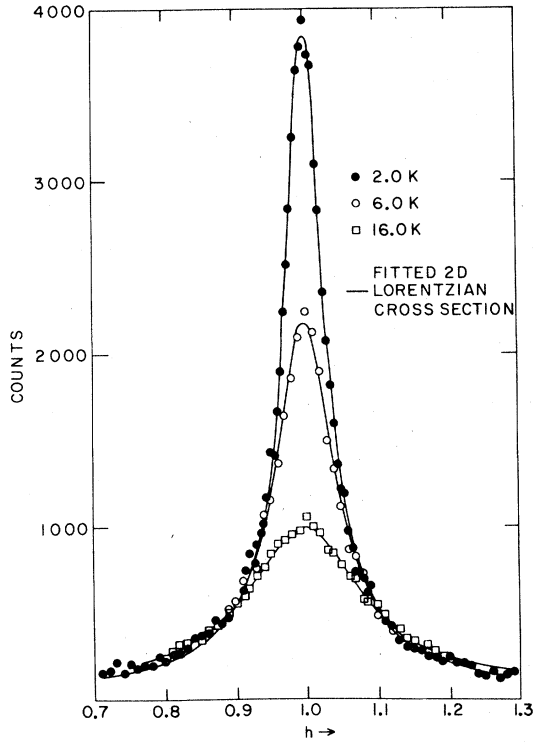


FIG. 10. Critical-scattering scans across the ridge at $(h, 0, 0.4)$ in $Rb_2Mn_{0.54}Mg_{0.46}F_4$ at several temperatures. The horizontal instrumental resolution is 0.011 $h$, FWHM. The solid lines are the fitted 2-D Lorentzians as discussed in the text.

We have fitted in a least-squares sense all of the data for the $c = 0.54$ and $c = 0.57$ samples to the single Lorentzian, Eq. (24), convoluted with the instrumental resolution function. The solid lines in Fig. 10 represent the results of such fits; it is clear that Eq. (24) describes the data quite well; $\chi^2$ is between 1 and 1.5 for most temperatures; at the minimum this demonstrates that it is not possible to extract $\mathcal{S}^{\parallel}$ and $\mathcal{S}^{\perp}$ separately from these data. The results for the inverse correlation length $\kappa$ and the peak intensity $\mathcal{S}(0) = A/\kappa^2$ are shown in Figs. 8 and 9. Again these results correspond quite well to our qualitative expectations based on the magnetic percolation theory summarized in Sec. III B. Both samples have $c < c_p$ so that no phase transitions to LRO is expected and none is observed. Rather both the correlation length and the structure factor saturate at finite values at the lowest temperature. Further these limiting values

are much larger in the 57% sample compared with the 54% sample as expected since the 57% sample is much closer to the percolation concentration $c_p = 0.593$. The $T = 0$ limiting widths are plotted versus concentration in Fig. 2, together with results obtained for the isostructural Ising system $Rb_2Co_cMg_{1-c}F_4$.[18] As we noted previously, all of the data fall on a simple smooth curve, albeit with quite generous error limit.

We shall postpone our quantitative analysis and discussion of these results to Sec. V. We now proceed to discuss some high-resolution energy analysis measurements.

### 2. *Measurements with energy analysis*

Measurements were performed with energy analysis for two reasons: first to examine the extent to which the magnetic behavior is dominated by the Heisenberg exchange interactions by separating the scattering into the two components $\mathcal{S}^{\parallel}(\vec{Q},\omega)$ and $\mathcal{S}^{\perp}(\vec{Q},\omega)$; second to examine the spectral form of $\mathcal{S}^{\parallel}(\vec{Q},\omega)$ and $\mathcal{S}^{\perp}(\vec{Q},\omega)$. In Paper I we have reported on measurements of $\mathcal{S}(\vec{Q},\omega)$ for energy transfers in excess of 1.0 meV. In this section we report on measurements at frequencies below 1.0 meV where the scattering is more specially characteristic of the percolation phenomena.

Since the measurements of the scattering for energy transfers below 1 meV require good energy resolution, the experiments were performed with incident neutrons of energy 5.0 meV, and a cooled Be filter was placed before the monochromator to filter the incident beam. The horizontal collimations used were 40 min throughout, and the energy resolution (FWHM) was 0.15 meV.

Measurements were made of the scattered intensity when the spectrometer was set to zero energy transfer; the intensity is then proportional to $I(\vec{Q},\omega)$ convoluted with the energy resolution, namely, the integral of $I(\vec{Q},\omega)$ for $|\omega|$ less than 0.075 meV. This quantity we denote as $I(\vec{Q},0)$, and the corresponding quantities for the scattering functions as $\mathcal{S}^{\parallel}(\vec{Q},0)$ and $\mathcal{S}^{\perp}(\vec{Q},0)$. $I(\vec{Q},0)$ was determined at a series of wave-vector transfers along the line in reciprocal space $(1,0,l)$. $\mathcal{S}^{\parallel}(\vec{q}^*,0)$ and $\mathcal{S}^{\perp}(\vec{q}^*,0)$ can then be obtained by plotting $I(\vec{Q},0)/|f(\vec{Q})|^2$ against $\sin^2\theta$ as shown in Fig. 11; $\vec{q}^*$ is the 2-D antiferromagnetic reciprocal-lattice vector. The results shown in Fig. 11 are reasonable straight lines and enable $\mathcal{S}^{\parallel}(\vec{q}^*,0)$ and $\mathcal{S}^{\perp}(\vec{q}^*,0)$ to be extracted separately, as shown in Fig. 12. At the highest temperature, 16.0 K, $\mathcal{S}^{\perp}(\vec{q}^*,0)$ is about one-half of $\mathcal{S}^{\parallel}(\vec{q}^*,0)$. On decreasing the temperature $\mathcal{S}^{\perp}(\vec{q}^*,0)$ has a maximum at about $7.5 \pm 2.0$ K where $\mathcal{S}^{\parallel}(\vec{q}^*,0)$ is about six times $\mathcal{S}^{\perp}(\vec{q}^*,0)$. On further decreasing the temperature, $\mathcal{S}^{\parallel}(\vec{q}^*,0)$ continues to increase until it becomes constant or almost constant at the lowest temperatures,

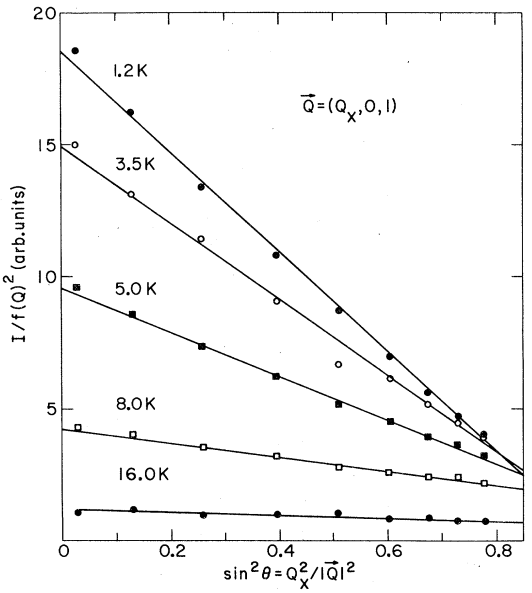


FIG. 11. Intensity variation $/|f(\vec{Q})|^2$ along the line $\vec{Q} = (Q_x, 0, 1)$ with the spectrometer set at $\omega = 0$, $\mathcal{S}(\vec{Q},0)$ for $Rb_2Mn_cMg_{1-c}F_4$. The solid lines are least-squares fits to the results with straight lines.

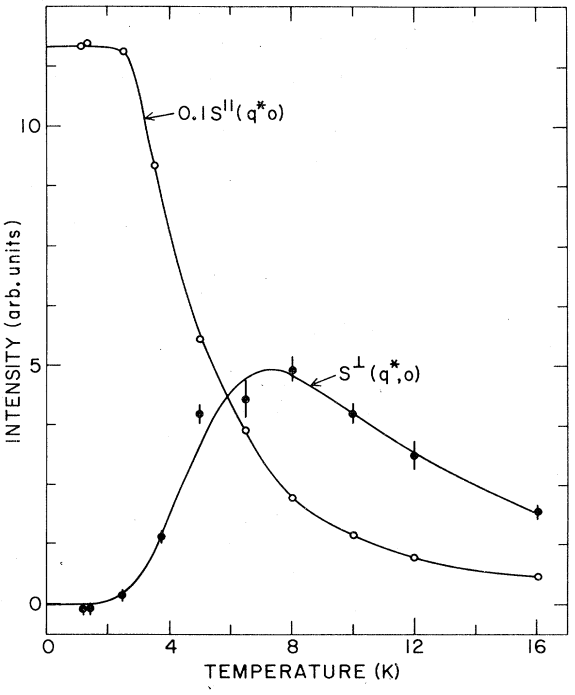


FIG. 12. $\mathcal{S}^{\parallel}(q^*,0)$ and $\mathcal{S}^{\perp}(q^*,0)$ for $Rb_2Mn_cMg_{1-c}F_4$ from the results shown in Fig. 7. Note the factor of 0.1 multiplying $\mathcal{S}^{\parallel}$.

while $\mathcal{S}^{\perp}(\vec{q}^*,0)$ decreases. In the $c=0.54$ specimen $\mathcal{S}^{\perp}(\vec{q}^*,0)$ decreases to nearly zero below 2.5 K while in the $c=0.57$ the decrease is less marked but the error bars become very large at low temperatures. The increase in the error bars arises partly because $\mathcal{S}^{\parallel}(\vec{q}^*,0)$ is larger than $\mathcal{S}^{\perp}(\vec{q}^*,0)$ by at least a factor of 100, but also because the width of the scattering in reciprocal space is comparable with the resolution function.

The differential scattering was measured using the constant $Q$ mode of operation for two different wave vectors $\vec{Q}=(1.0,0,0.4)$ and $(1.0,0,4.1)$. The scattering functions $\mathcal{S}^{\parallel}(\vec{q}^*,\omega)$ and $\mathcal{S}^{\perp}(\vec{q}^*,\omega)$ can then be obtained from these two measurements, given knowledge of the form factor,[41] and the geometrical factors. $\mathcal{S}^{\parallel}(\vec{q}^*,\omega)$ is shown in Fig. 13 for the $c=0.54$ specimen. At the lowest temperatures, $<5.0$ K, the scattering is almost entirely quasielastic with a width limited by the instrumental resolution. On increasing the temperature, the intensity of the central quasielastic peak continues to decrease while a broader inelastic component tends to increase until by 16.0 K the integrated intensity of the broader component is approximately twice that of the quasielastic peak. The *estimated* behavior of $\mathcal{S}^{\perp}(\vec{q}^*,\omega)$ is illustrated in Fig. 14. At the lowest temperatures it is erroneously negative at zero energy. This is because of subtle resolution effects not explicitly accounted for in this analysis. At somewhat larger frequencies

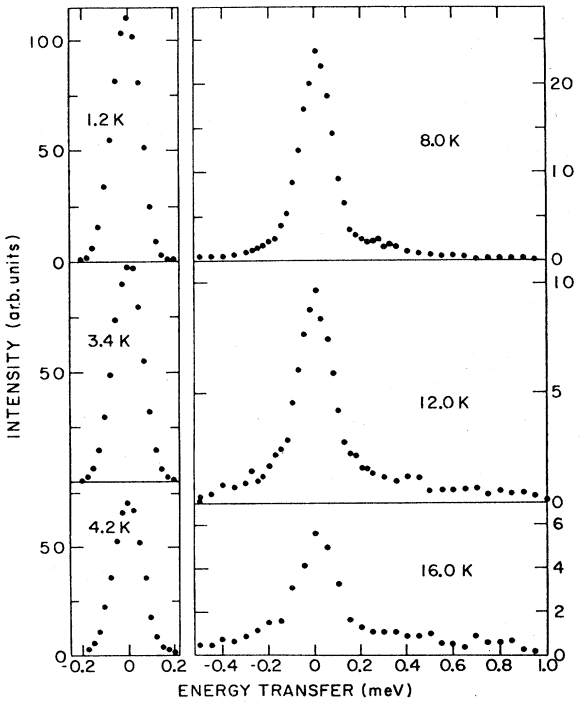


FIG. 13. Longitudinal correlation function, $\mathcal{S}^{\parallel}(q^*,\omega)$, for $Rb_2Mn_{0.54}Mg_{0.46}F_4$ at various temperatures.

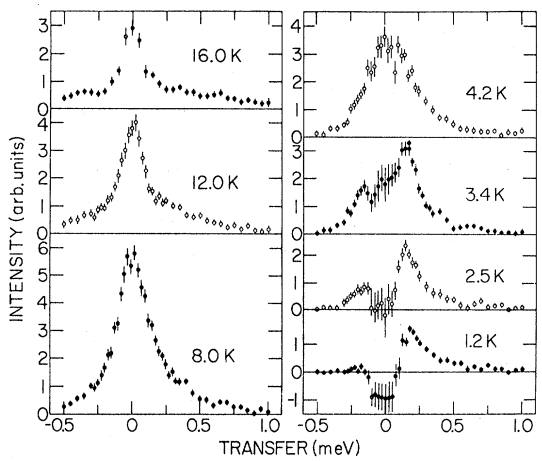


FIG. 14. Transverse correlation function, $\mathcal{S}^{\parallel}(q^*,\omega)$, for $Rb_2Mn_{0.54}Mg_{0.46}F_4$ at various temperatures.

the scattering shows some suggestion of an inelastic peak with an energy of $0.18\pm0.04$ meV. In pure $Rb_2MnF_4$ the dipolar anisotropy gives a spin-wave-energy gap of 0.602 meV.[1] On increasing the temperature the inelastic peak becomes more intense and there is evidence of its also occurring for neutron energy loss at 3.4 K. We should emphasize, however, that these spectra involve taking the differences of two large numbers near $E=0$ so that large errors may result. Indeed EPR measurements by Walsh *et al.*[42] show that at 1.7 K there is still significant weight in $\chi^{\perp}(\omega)$ for $E<0.1$ meV. At higher temperatures the elastic scattering increases until at 16.0 K it is very similar in form to $\mathcal{S}^{\parallel}(\vec{q}^*,\omega)$ except that the ratio of the intensity of the broad component to the quasielastic component is larger in $\mathcal{S}^{\perp}(\vec{q}^*,\omega)$ than $\mathcal{S}^{\parallel}(\vec{q}^*,\omega)$.

Similar measurements were carried out for the $c=0.57$ specimen, but the uncertainties caused by the resolution effects were more significant than for the $c=0.54$ specimen. This was especially the case at low temperatures. At higher temperatures the spectra for $c=0.57$ were quantitatively very similar to those shown in Figs. 13 and 14.

## V. ANALYSIS AND DISCUSSION

It is evident that many of the qualitative features anticipated from the magnetic percolation theory discussed in Sec. III are indeed observed in the system $Rb_2Mn_cMg_{1-c}F_4$. In this section we shall give a more quantitative comparison with the theory. We have already discussed the results for the 60% sample extensively in Sec. IV A. We concentrate here on the results for the 54% and 57% samples.

As discussed in Sec. III, at low temperatures the measured $S(\vec{Q})$ is expected to be characteristic of the

pure percolation problem. The inelastic measurements show that for $T \leq 3$ K the spins are essentially frozen along the $z$ axis; indeed this is shown with rather more accuracy by the EPR measurements of Walsh *et al.*,[42] which indicate that the spins are static on a time scale of greater than $10^{-8}$ seconds at 1.7 K. In this limit, $I(\vec{Q})$ at $T \lesssim 3$ K then measures simply the Fourier transform of the two-particle distribution function $C_2(\vec{r})$. We find that the low-temperature profiles are adequately described by Lorentzians for $c = 0.54$ and $c = 0.57$. Similar results are found in $Rb_2Co_cMg_{1-c}F_4$ for all concentrations $< c_p$. This in turn implies that

$$C_2(r) \sim e^{-\kappa_G r}/r^{1/2} \ , \tag{25}$$

in agreement with the percolation theory. We note that our experiments are not accurate enough to measure any subtle deviations from Eq. (10), which should appear sufficiently close to the percolation point.

The geometrical inverse-correlation lengths so obtained are shown for our samples of $Rb_2Mn_cMg_{1-c}F_4$ and $Rb_2Co_cMg_{1-c}F_4$ in Fig. 2. According to percolation theory, one should have

$$\kappa(\Delta c, 0) = \kappa_G = \kappa_G^0 (1 - c/0.593)^{1.35} \ .$$

We have chosen $\kappa_G^0 = 3$ to give the best mean fit to the data. It is evident from Fig. 2 that the above equation describes the experimental data remarkably well. Indeed the fit is very much better than the apparent uncertainties in the concentrations. To a certain extent, we have biased the agreement by using as the center of the error bars for the Co compound the results of the chemical analyses, which are no more reliable than the lattice constants or the starting concentrations as an indicator of the true composition. We should re-emphasize however that all of these values are included by the indicated error limits. We note that, as far as we know, there is as yet no theoretical value for $\kappa_G^0$ for the site-random nn square-lattice problem. Clearly, a theoretical calculation of $\kappa_G^0$ to compare with our experiments would be most valuable.

We now consider the temperature dependence of the inverse correlation length $\kappa(\Delta c, T)$ and the structure factor $S(\Delta c, T, 0)$. It is clear qualitatively from Fig. 8 that the $c = 0.54$ and $c = 0.57$ data are well described by the heuristic relationship $\kappa(\Delta c, T) = \kappa(\Delta c, 0) + \kappa(0, \mu)$, that is, a $T = 0$ part and a temperature-dependent part. As we shall see in Paper III similar results are obtained in $Rb_2Co_cMg_{1-c}F_4$. We have therefore fitted the data at both concentrations to the form

$$\kappa = \kappa_G + \alpha \kappa_1^{\parallel}(T)^{\nu_T} \ , \tag{26}$$

where $\kappa_G = \kappa(\Delta c, 0)$. Clearly our use of $\kappa_1^{\parallel}(T)$ as the temperature scaling field is only approximate for two principal reasons: (i) the data actually measure the combination given by Eq. (25), so that one should really have a theoretical cross section for this combination; from Fig. 5, however, it is apparent that for $T \gtrsim 10$ K, $\kappa^{\parallel} \simeq \kappa^{\perp}$ so that Eq. (26), should be completely adequate in this temperature range; similarly, for $T \leq 5$ K, we expect $S^{\parallel}$ to dominate $I(\vec{Q})$ completely so that in this regime one must use $\kappa_1^{\parallel}(T)$. (ii) $\kappa_1^{\parallel}(T)$ has been calculated using the Blume *et al.*[34] classical linear-chain model; the experiments in $Mn_cZn_{1-c}F_2$ suggest that this classical model underestimates the effect of the anisotropy; this will only affect the detailed temperature dependence in the crossover region and should not affect the data above 10 K or below 5 K.

Because of the above caveats we have excluded the data between 5 and 10 K from the fits to Eq. (26). The results of the fits are shown as the solid lines in Fig. 8. It is evident that Eq. (26) describes the measurements extremely well even in the 5 − 10 K crossover region. We remind the reader that in one dimension Eq. (26) is exact with $\alpha = 1$ and $\nu_T = 1$. In this case from our best fits we find $\alpha = 1.0 \pm 0.05$ and $\nu_T = 0.90 \pm 0.05$ for $Rb_2Mn_cMg_{1-c}F_4$. We should note that in a previous publication[5] we suggested a value of $\nu_T = 0.75 \pm 0.05$. However, that analysis did not take into account explicitly the limiting inverse correlation length at $T = 0$ due to the finite cluster size for $c < c_p$; that is, it effectively assumed $\kappa_G = 0$. Accordingly, the exponent $\nu_T$ was underestimated. We believe, therefore, that our current value $\nu_T = 0.90 \pm 0.05$ is to be preferred. We shall discuss the significance of this value for $\nu_T$ below.

In order to extract a structure-factor temperature exponent $\gamma_T$ it is also necessary to incorporate the effects of finite cluster size. We have suggested in Sec. III, in the absence of any rigorous theory, that one may write

$$S(\Delta c, \mu, 0) \sim \kappa^{-(2-\eta)} \ , \tag{27}$$

with $\kappa$ given by Eq. (26). This will then give $\gamma_T = \nu_T(2-\eta)$. Accordingly we have fitted the measured data to Eq. (27) using the empirically measured $\kappa$. The results are shown as the solid lines in Fig. 9. It is evident that Eq. (27) describes the data reasonably well, although the effective $\eta$ seems to be somewhat concentration dependent. We shall use the value obtained from the 57% sample since it is somewhat closer to the percolation threshold. This analysis gives $\gamma_T = 1.50 \pm 0.15$. We thus have finally for $\gamma$ and $\nu$ for the percolation multicritical exponents in the 2-D near-Heisenberg magnet

| | Percolation | Temperature |
|---|---|---|
| $\nu$ | $1.354 \pm 0.015$ | $0.90 \pm 0.05$ |
| $\gamma$ | $2.432 \pm 0.035$ | $1.50 \pm 0.15$ |

According to the $\phi = 1$ theories the percolation and

temperature exponents should be identical. Our experiments instead suggest a crossover exponent $\phi = 1.5 \pm 0.15$. We should note that the SAW[6] model gives $\phi = 1.7$, a value rather close to the experiments; at this point, this latter model is largely heuristic; clearly more theoretical work on the SAW approach would be most valuable. As we discussed in Sec. III, the theory for the the percolation multicritical point in the 2-D Ising model which gives $\phi = 1$ is believed to be exact. Indeed, this latter result and the disagreement with the $Rb_2Mn_cMg_{1-c}F_4$ results have motivated us to carry out experiments on the 2-D Ising system $Rb_2Co_cMg_{1-c}F_4$. We show the results for $\kappa$ for $Rb_2Co_{0.575}Mg_{0.425}F_4$ in Fig. 15 together with our results in the $c = 0.57$ sample. In order to compare these results quantitatively it is necessary to plot them versus $\kappa_1^{\parallel}(T)$, the 1-D correlation length. It is evident that on this temperature scale, at high temperatures the correlation lengths in the Ising and Heisenberg system are quite similar, as one would intuitively expect. However, the evolution with decreasing $\kappa_1(T)$ is distinctly different. Indeed the Ising system turns out to be well described by the percolation exponents, as we shall discuss in Paper III.

We believe, therefore, that, in two dimensions, there is an essential difference between the Ising and near-Heisenberg systems. Presumably this difference originates in the extended nature of the low-energy excitations in the Heisenberg system. Indeed, one might argue that, in the Ising system, one may break the coordination between two parts of a cluster either by removing a spin or by a thermal excitation at a particular site. Both are local effects which, if equivalent, would suggest $\phi = 1$. However, for the Heisenberg system the geometrical "excitations" are local, whereas the thermal excitations are extended. Indeed, if we assume that the long-wavelength excitations in the Heisenberg system propagate primarily along the backbone of the cluster, then we might expect the crossover exponent to be determined by the effective dimensionality of the backbone. An essential underlying assumption of the SAW ansatz as originally used by us[1] and by Stanley *et al.*[7] is that this backbone has the fractal dimensionality[43] of an SAW. Recent calculations by Halley and Mai[44] on the square lattice at $c = c_p$ have verified that this is, in fact, the case.

Clearly more theory is required for the Heisenberg model. Nevertheless, our overall picture of magnetic behavior near the percolation multicritical point seems to be quite good. Indeed the progress which has been achieved since our original publication has been quite gratifying. We hope that these results will stimulate further theory on this most interesting problem.

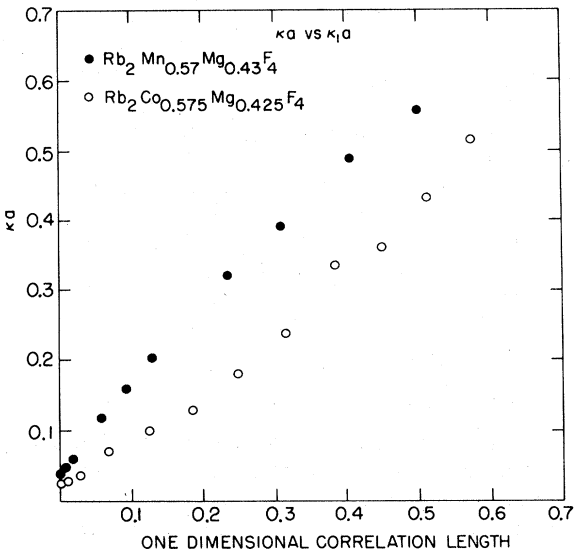


FIG. 15. Measured inverse correlation lengths in $Rb_2Mn_{0.57}Mg_{0.43}F_4$ and $Rb_2Co_{0.575}Mg_{0.425}F_4$ vs the underlying one-dimensional correlation lengths. For the Mn compound $\kappa_1(T)$ is taken from Fig. 5 while for the Co compound $\kappa_1(T) = \ln(\tanh \mathcal{J}/t)$ with $\mathcal{J} = 42$ K.

## ACKNOWLEDGMENTS

We would like to acknowledge stimulating conversations about this work with M. Blume, G. Grest, S. Kirkpatrick, W. Klein, T. C. Lubensky, P. Reynolds, M. J. Stephen, and M. Wortis. We are very grateful to M. E. Fisher, H. E. Stanley, and P. W. Stephens for helpful comments on the manuscript and for interesting discussions. The work at M. I. T. was supported by the NSF Materials Research Laboratory Grant No. DMR-76-80895. Research at Brookhaven was supported by the Division of Basic Energy Sciences, DOE, under Contract No. EY-76-C-02-0016.

---

*Guest Scientist, BNL, Upton, N. Y.
†Permanent address: Dept. of Phys., Univ. of Edinburgh, Edinburgh, Scotland.
‡Present address: K. M. S. Fusion Inc., Ann Arbor, Mich. 48106.

[1]R. A. Cowley, G. Shirane, R. J. Birgeneau, and H. J. Guggenheim, Phys. Rev. B 15, 4292 (1977).
[2]For a review see R. A. Cowley, in *Proceedings of the 21st Conference on Magnetism and Magnetic Materials, 1975,* edited by J. J. Becker, G. H. Lander, and J. J. Rhyne, AIP Conf. Proc. No. 29 (AIP, New York, 1976), p. 243.
[3]For reviews see V. K. S. Shante and S. Kirkpatrick, Adv.

Phys. 20, 325 (1971); J. W. Essam, in *Phase Transitions and Critical Phenomena,* edited by C. Domb and M. S. Green (Academic, New York, 1972), Vol. II, p. 197.
[4]S. Kirkpatrick, Phys. Rev. Lett. 36, 69 (1976).
[5]R. J. Birgeneau, R. A. Cowley, G. Shirane, and H. J. Guggenheim, Phys. Rev. Lett. 37, 940 (1976).
[6]D. Stauffer, Z. Phys. B 22, 161 (1976).
[7]H. E. Stanley, R. J. Birgeneau, P. J. Reynolds, and J. F. Nicoll, J. Phys. C 9, L553 (1976).
[8]T. C. Lubensky, Phys. Rev. B 15, 311 (1977).
[9]M. J. Stephen and G. S. Grest, Phys. Rev. Lett. 38, 567 (1977).
[10]D. J. Wallace and A. P. Young, Phys. Rev. B 17, 2384 (1978).
[11]T. K. Bergstresser, J. Phys. C 11, 3831 (1977).
[12]E. Domany, J. Phys. C 11, L337 (1978).
[13]R. Bibaux, J. P. Carton, and G. Sarma, J. Phys. A 9, L87 (1976).
[14]S. Kirkpatrick, Phys. Rev. B 15, 1533 (1977).
[15]E. F. Shender, J. Phys. C 9, L309 (1976).
[16]R. B. Stinchcombe, J. Phys. C 12, L41 (1979).
[17]C. Jayaprakash, E. K. Riedel, and M. Wortis, Phys. Rev. B 18, 2244 (1978).
[18]R. A. Cowley, G. Shirane, R. J. Birgeneau, H. J. Guggenheim, and H. Ikeda (unpublished).
[19]P. J. Reynolds, H. E. Stanley, and W. Klein, J. Phys. A 11, L199 (1978).
[20]W. Marshall and S. W. Lovesey, *Theory of Thermal Neutron Scattering* (Oxford University, New York, 1971).
[21]P. J. Reynolds, H. E. Stanley, and W. Klein, J. Phys. A 10, L203 (1977).
[22]W. Klein, H. E. Stanley, P. J. Reynolds, and A. Coniglio, Phys. Rev. Lett. 41, 1145 (1978); J. Blease, J. W. Essam, and C. M. Place, J. Phys. C 11, 4009 (1978); D. S. Gaunt and H. Rushkin, J. Phys. A 11, 1369 (1978); P. J. Reynolds (private communication).
[23]P. W. Kasteleyn and C. M. Fortuin, J. Phys. Soc. Jpn. Suppl. 26, 11 (1969).
[24]R. J. Elliott, B. R. Heap, D. J. Morgan, and G. S. Rushbrooke, Phys. Rev. Lett. 5, 366 (1960).
[25]R. A. Cowley, G. Shirane, R. J. Birgeneau, and E. C. Svensson, Phys. Rev. Lett. 39, 894 (1977).
[26]A. B. Harris, J. Phys. C 7, 1671 (1974).
[27]R. J. Birgeneau, J. Als-Nielsen, and G. Shirane, Phys. Rev. B 16, 280 (1977).
[28]M. F. Thorpe, J. Phys. (Paris) 36, 117 (1975).
[29]See for example, J. Als-Nielsen and R. J. Birgeneau, Am. J. Phys. 45, 554 (1977).
[30]M. E. Fisher and J. W. Essam, J. Math. Phys. 2, 609 (1961).
[31]P. W. Anderson (private communication).
[32]C. Domb, Adv. Chem. Phys. 15, 229 (1964).
[33]R. J. Birgeneau, J. Skalyo Jr., and G. Shirane, J. Appl. Phys. 41, 1303 (1970); Phys. Rev. B 3, 1736 (1973); H. E. Stanley and T. Kaplan, Phys. Rev. Lett. 17, 913 (1966).
[34]M. Blume, P. Heller, and N. A. Lurie, Phys. Rev. B 11, 4483 (1975).
[35]D. J. Breed, K. Gilijamse, J. W. E. Sterkenburg, and A. R. Midiema, J. Appl. Phys. 41, 1267 (1970).
[36]Ref. 3 and S. Kirkpatrick (private communication)
[37]R. J. Birgeneau, H. J. Guggenheim, and G. Shirane, Phys. Rev. B 1, 2211 (1970); 8, 304 (1973).
[38]D. E. Cox, G. Shirane, R. J. Birgeneau, and J. B. MacChesney, Phys. Rev. 188, 930 (1969).
[39]D. E. Moncton, F. J. DiSalvo, J. D. Axe, L. J. Sham, and B. R. Patton, Phys. Rev. B 14, 3432 (1976); L. Bevaart, F. Frikkee, J. V. Lebesque, and L. J. de Jongh, Phys. Rev. B 18, 3376 (1978); E. J. Samuelsen, J. Phys. Chem. Solids 35, 785 (1974); H. Ikeda, M. T. Hutchings, and M. Suzuki, J. Phys. C 11, L359 (1978).
[40]J. Als-Nielsen, R. J. Birgeneau, H. J. Guggenheim, and G. Shirane, Phys. Rev. B 12, 4963 (1975).
[41]R. E. Watson and A. J. Freeman, Acta Crystallogr. 14, 27 (1961).
[42]W. M. Walsh Jr., R. J. Birgeneau, L. W. Rupp Jr., and H. J. Guggengeim Phys. Rev. B 20, 4645 (1979).
[43]H. E. Stanley, J. Phys. C 11, L211 (1977).
[44]J. W. Halley and Thang Mai, Phys. Rev. Lett. 43, 740 (1979). These authors suggest that in Refs. 5 and 7 it was not entirely clear which aspect of the large percolation clusters the SAW was meant to represent. Our statement in Ref. 5 "the longest paths across the cluster simulate self-avoiding walks on a square lattice" was meant explicitly to identify the backbone of the cluster with an SAW. We trust that this statement plus our discussion in this paper removes any possible ambiguities.